chemosensors

MDPI

Article

Adamantane Three-Dimensional Porous Organic Framework as a Fluorescence Sensor for Rapid Determination of Tetracycline in Aquatic Products

Zhenyu Lu, Yufei Hu, Gongke Li * and Ling Xia *

School of Chemistry, Sun Yat-Sen University, Guangzhou 510006, China
* Correspondence: cesgkl@mail.sysu.edu.cn (G.L.); xialing@mail.sysu.edu.cn (L.X.)

Abstract: A fluorescence adamantane three-dimensional porous organic framework (AdaPOF) was synthesized via a Suzuki coupling reaction. The AdaPOF showed excellent fluorescence performance with a relative high quantum yield and fluorescence stability. Due to its excellent selectivity to tetracycline (TC), a fluorescence sensor based on AdaPOF was constructed for TC determination. The selective sensing mechanism of the AdaPOF towards TC was studied by density functional theory (DFT) calculation experiments. An AdaPOF–based fluorescence method for TC determination was established, with the linear range of 0.1–9.0 μmol/L (R^2 = 0.9959) and the limit of detection (*S/N* = 3) of 43 nmol/L. Moreover, the fluorescence method was used to the determination of TC in aquatic products and the recoveries were ranged from 94.4% to 103.8%. The results obtained by this fluorescence method were consistent with those of the high-performance liquid chromatography (HPLC) method in the TC determination.

Keywords: adamantane; porous organic framework; tetracycline; fluorescence sensor; aquatic products

Citation: Lu, Z.; Hu, Y.; Li, G.; Xia, L. Adamantane Three-Dimensional Porous Organic Framework as a Fluorescence Sensor for Rapid Determination of Tetracycline in Aquatic Products. *Chemosensors* **2022**, *10*, 457. https://doi.org/10.3390/chemosensors10110457

Academic Editor: Chung-Wei Kung

Received: 27 September 2022
Accepted: 2 November 2022
Published: 4 November 2022

1. Introduction

Tetracycline (TC) is a kind of broad-spectrum antibiotic produced by actinomycetes which has the advantage of low toxicity and easy absorption, meaning it is widely used in the treatment of bacterial infections [1,2]. In addition, TC is also widely used in animal feed as a drug additive to prevent bacterial infection and promote growth [3]. However, the overuse or abuse of TC can cause bacterial resistance and create drug residues in animals. Food pollution caused by TC residues not only seriously threatens human health, but also has a huge impact on international trade. The illegal use of TC will also bring serious pollution to the ecological environment [4]. Therefore, there is a strong need to establish an analytical method for the determination of TC.

Several analytical methods have been developed for TC determination, including high-performance liquid chromatography [5], high-performance liquid chromatography tandem mass spectrometry [6] and the capillary electrophoresis method [7]. Although these methods have high sensitivity and accuracy, they often suffer from time-consuming, complicated experimental processes or the requirement of expensive equipment. Fluorescence methods have attracted widespread attention due to their advantages of a fast response, high sensitivity and simple equipment [8–10]. The fluorescence material plays an important role in the sensitivity, selectivity and sensing speed of a fluorescence method [11,12]. There are some reports on the determination of TC by sensors based on fluorescence materials, such as carbon dots [13], Eu^{3+}-functionalized silicon nanoparticles [14] and SYBR Green I [15]. However, these methods have the disadvantages of poor selectivity and reusability. Consequently, synthesis of new fluorescent materials to establish a fluorescence method with a fast response, high sensitivity and repeatability is of great significance.

Porous organic frameworks (POFs) are a new kind of material formed by the coupling or condensation reaction of organic precursors based on light elements, such as C, B, H,

O and N [16–18]. It has great advantages in the application of fluorescence sensing. For example, there are many delocalized π electrons in the framework, and its porous structure can reduce fluorescence self-quenching behavior by promoting electron migration [19]. In addition, POFs also has good stability and performance in being reused [20]. However, the reported fluorescence sensor-based POFs are usually constructed by two-dimensional POFs [21]. Compared with two-dimensional POFs, three-dimensional POFs have larger surface area, more interconnected channels, superior stability and fully exposed active sites [22–24], thus having greater application potential in the field of fluorescence sensing.

In this work, a fluorescence three-dimensional adamantane porous organic framework (AdaPOF) was prepared by a polymerization reaction of 1, 3, 5, 7–tetrakis(4–bromophenyl) adamantane (TBPA) and 1, 3, 5–tri (4–pinacholatoborolanephenyl) benzene (TPPB). The prepared AdaPOF had excellent fluorescence properties, and a fluorescence sensor based on AdaPOF was fabricated for selective determination of TC. Moreover, we have expounded the quenching mechanism of this fluorescence sensor by a fluorescence lifetime assessment and UV–vis spectra. Additionally, the AdaPOF–based fluorescence sensor was further used to detect TC residues in aquatic products.

2. Materials and Methods

2.1. Materials and Reagents

TBPA, TPPB, tetrakis (triphenylphosphine) palladium (0) (Pd ≥ 8.9%), glucose, urine, Vitmorningin B1, Vitamin C were purchased from Aladdin Chemistry Co., Ltd. (Ontario, CA, USA) Potassium carbonate (K_2CO_3), tetracycline, chlortetracycline, oxytetracycline, roxithromycin, sulfadiazine, metronidazole, ornidazole, thiabendazole, thiamphenicol and sulfamethazine were purchased from J&K Scientific. All other reagents were obtained from the Guangzhou chemical reagent factory.

2.2. Instruments

Nuclear magnetic resonance spectroscopy data were assessed with a Bruker 400 MHz NMR spectrometer. Thermogravimetric analysis was obtained on a NETZSCH TG 209 F1 Libra under the temperature range of room temperature to 90 °C under nitrogen conditions. Scanning electron microscopy was conducted on a field emission SEM 500 scanning electron microscope. Transmission electron microscopy was conducted on a FEI Tecnai G2 F30–300 KV transmission electron microscope. N_2 sorption isotherms were obtained on a Micromeritics ASAP 2460 surface area and pore size analyzer. UV–vis spectra were carried out on a Shimadzu UV–2600 spectrophotometer. Fluorescence spectra were carried out on a Shimadzu RF-5301PC fluorescence spectrophotometer.

2.3. Synthesis of Adamantane Porous Organic Framework

AdaPOF was prepared via Suzuki coupling reactions [25]. Briefly, TBPA (500 mg, 0.66 mmol), TPPB (603 mg, 0.88 mmol), K_2CO_3 (1.33 g, 9.6 mmol) and $Pd(PPh_3)_4$ (Pd ≥ 8.9%, 34.8 mg, 0.03 mmol) were added into a mixed solution of DMF (15 mL) and water (1 mL). Subsequently, the mixed solution was degassed with nitrogen protection. The solution was then heated up to 15 °C for 3 d. When the reaction was over, 200 mL of water was added into the mixed solution. The gray precipitate was obtained by filtration, and it was further washed with HCl, water, tetrahydrofuran and dichloromethane in sequence. Finally, the precipitate was collected after drying in vacuum and was named AdaPOF.

2.4. Fluorescence Measurements

A total of 15 mg of AdaPOF and 50 mL of anhydrous dichloromethane were placed in a volumetric flask and the solution was formed a suspension by ultrasound for 4 h. The obtained suspension of AdaPOF suspension was then diluted with anhydrous dichloromethane to 100 mL. The fluorescence measurements were carried out as follows: 2.7 mL of the AdaPOF suspension was added to a quartz cuvette, then 0.3 mL of different concentrations of TC were added to the quartz cuvette, and the final concentrations of TC in quartz cuvette were 0, 0.1,

0.3, 0.5, 0.8, 1.0, 3.0, 5.0, 7.0 and 9.0 μmol/L. The fluorescence intensity of the above mixed solution was assessed in a range from 350 to 500 nm at 334 nm excitation wavelength and a slit width of 5 nm.

The calculated method of the LOD is listed in the supporting information.

2.5. DFT Calculations

The DFT calculations, the B3LYP/6–31G* basis set in Gaussian 09 [26], were performed to optimize geometries and evaluate the LUMO and HOMO energies of AdaPOF and analytes.

2.6. Sample Preparation

The samples of fish, shrimp and crab were purchased at a farmers' market. The sample preparation processes were as follows: 5.0 g of sample and 10 mL of perchloric acid solution (0.5%) were placed in a test tube. After ultrasonication and shaking extraction, the supernatant was obtained by centrifugation. The residue was further extracted with perchloric acid solution (0.5%, volume fraction), and the above operations were repeated. Finally, this was combined with the supernatant. The obtained supernatant was placed in an *n*-hexane solution. After shaking for 5 min, the aqueous phase was obtained by centrifugation (3000 r/min) and pretreated with an ODS–C18 column. The column was subsequently eluted using a methanol solution and the eluent was collected. Finally, the eluent solution was evaporated to dryness and dissolved with 1 mL of methanol solution for later use.

3. Results

3.1. Characterization of AdaPOF

AdaPOF was prepared by the Suzuki coupling reaction of TPPB and TBPA in a mixed solution of DMF and water (Figure 1). The morphology of the as–prepared AdaPOF was characterized by scanning electron microscopy (SEM) and transmission electron microscope (TEM) images. The SEM image of Figure 2a showed that the AdaPOF exhibited spherical structure, an effect which may be caused by the agglomeration of small particles and the diameter of small spheres being in the range of 65 to 70 nm. The TEM image of Figure 2b revealed that the AdaPOF had an amorphous porous structure [25].

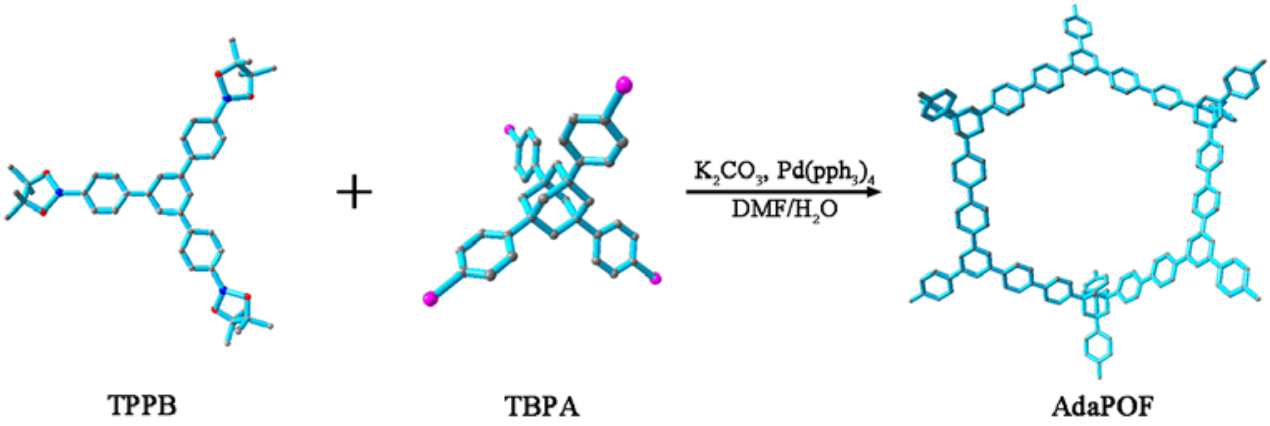

Figure 1. Synthesis routine of AdaPOF.

Fourier transform infrared spectroscopy (FT–IR) was performed to study the compositional and functional groups of AdaPOF. As show in Figure 2c, the peaks at 2925 and 2852 cm^{-1} can be assigned to $–CH_2–$ stretching vibration; the peaks obtained at 1596 and 1078 cm^{-1} represent the stretching vibration of the C=C on the benzene ring (curve 1). These results indicated that there were a large number of methylene and benzene rings in the AdaPOF framework. In addition, the characteristic of C-Br stretching bands (532 cm^{-1}), only observed in the TBPA framework [27] (curve 2) with none in the frameworks of

TPPA (curve 3) and AdaPOF, revealed that the AdaPOF had been successfully prepared by TBPA and TPPA. Raman spectra were used to further characterize the materials. Figure 2d showed that only TBPA had a strong Raman peak of C–Br at 1023 cm^{-1} [28] (curve 2), while AdaPOF (curve 1) and TPPA (curve 3) had no peak at this position. These characterizing results further proved the successful synthesis of the AdaPOF. A solid−state ^{13}C CP/MAS NMR spectrum was also measured to investigate structural information of AdaPOF at molecular level. As showed in Figure S1, the peaks at 39.5 and 46.1 ppm were assigned to the carbon atom signal of adamantane, the peaks at 127.6 and 141.2 ppm could be ascribed to some carbon atom signals on the benzene ring of TBPA and TPPA, and the peaks at 148.8 ppm were assigned to the carbon atom signal of benzene ring connected with adamantane. The X–ray diffraction (XRD) measurement of AdaPOF only showed the broad and scattered characteristics and no obvious peaks were found (Figure S2), revealing that the as–prepared AdaPOF had an amorphous structure [29].

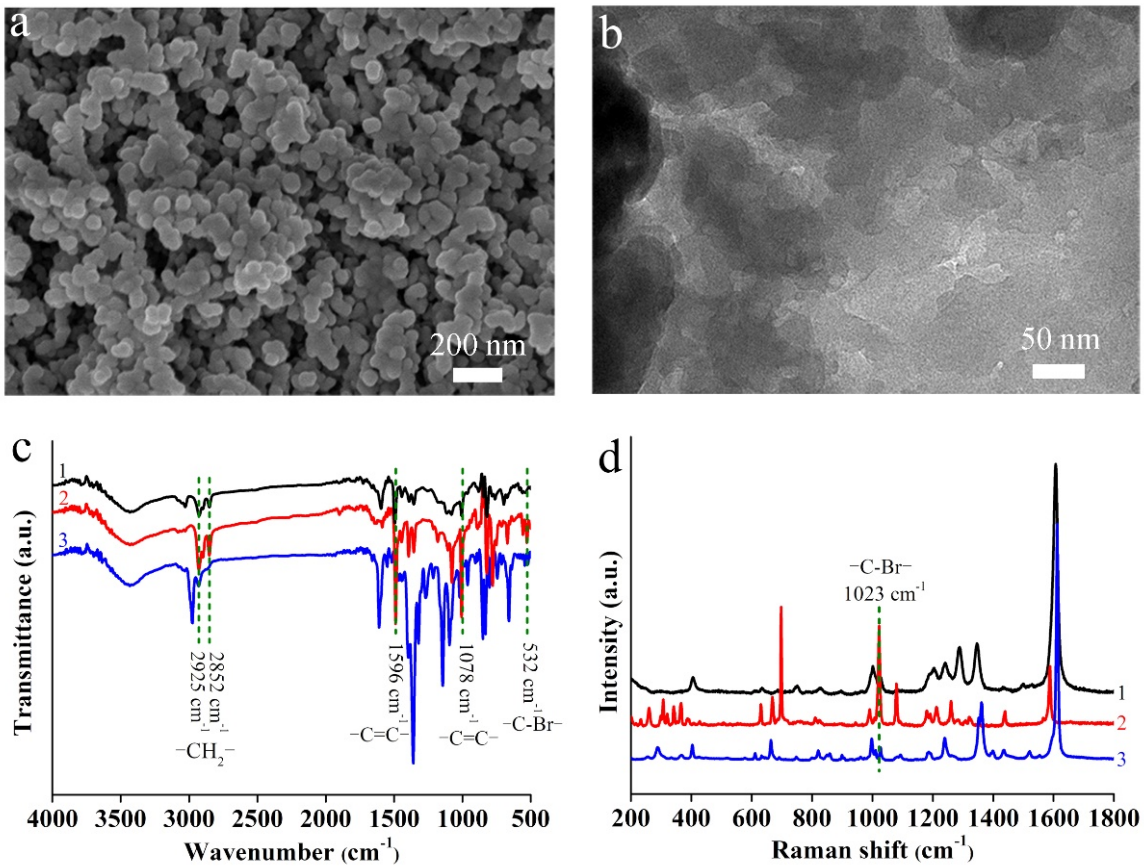

Figure 2. (**a**) SEM and (**b**) TEM images of AdaPOF; (**c**) FT–IR spectra of AdaPOF; (**d**) Raman spectra of AdaPOF.

The porous property of the AdaPOF was assessed by the N_2 adsorption–desorption experiments at 77 K. As shown in Figure S3a, the adsorption curve of the AdaPOF had a feature of type II N_2 adsorption isotherm and the curve rose steeply at the lower pressure region, revealing that the material had the characteristics of microporous structure. Figure S3a illustration revealed that the pore size of the AdaPOF was mainly distributed in the range of micropore (<2 nm), which was consistent with the characterization of the adsorption curve. The Brunauer–Emmett–Teller surface area of AdaPOF was calculated to be 546 m^2/g, and the pore volume was determined to be 0.12 cm^3/g. The thermogravimetric analysis of AdaPOF observed that the material has good thermal stability at 485 °C (Figure S3b).

3.2. Performance of AdaPOF–Based Fluorescence Sensor

The fluorescence spectra of AdaPOF were recorded and shown in Figure S4. The AdaPOF suspension possessed a fluorescence emission peak at 380 nm with an excitation wavelength at 334 nm. Figure S4 illustrations showed that the suspension of AdaPOF exhibited off–white coloring under sunlight and exhibited blue under 365 nm UV–light. The quantum yield of AdaPOF suspension was studied by quinine sulfate in 0.1 mol/L H_2SO_4 as the standard (54%). The relative quantum yield of AdaPOF was calculated to be 5.9%. The AdaPOF suspension displayed a well fluorescence stability for 30 min and 7 d (Figure S5a,b). The suspension of AdaPOF prepared in the same and different batches also showed excellent fluorescence stability (Figure S5c,d). These characteristics showed that the AdaPOF had good fluorescence properties, which laid a foundation for further fluorescence sensing.

The fluorescence sensing performance of the AdaPOF–based sensor to TC was investigated by adding various concentrations (0.1, 0.5 and 1.0 μmol/L) of TC standard solution to the AdaPOF suspension. Figure 3a showed that the fluorescence intensity of AdaPOF at 380 nm decreased with the addition of a TC methanol solution. Moreover, the fluorescence intensity of AdaPOF gradually decreased as the concentration of TC methanol solution increased. Moreover, the methanol blank solvent had a negligible effect on the fluorescence intensity of the AdaPOF (Figure S6). The results reveal that the AdaPOF–based sensor could be used for TC detection. In order to study the selectivity performance of the sensor based on AdaPOF to TC, the fluorescence quenching effect of the sensor was recorded by adding seven common antibiotics (c = 1.0 μmol/L), including methacycline, tigecycline, demeclocycline, doxycycline, oxytetracycline, thiamphenicol, ampicillin, roxithromycin, thiabendazole, sulfadiazine and sulfamethazine. Figure 3b showed that obvious fluorescence quenching effects were obtained after adding TC and its structural analogues, such as methacycline, tigecycline, demeclocycline, doxycycline and oxytetracycline. In addition, when adding some classes of other antibiotics, such as thiamphenicol, ampicillin, roxithromycin, thiabendazole, sulfadiazine and sulfamethazine, no obvious fluorescence quenching effects were obtained in response to AdaPOF suspension. These results revealed that the AdaPOF–based sensor could not distinguish TC from its structural analogues, but had good selectivity towards TC from other antibiotics.

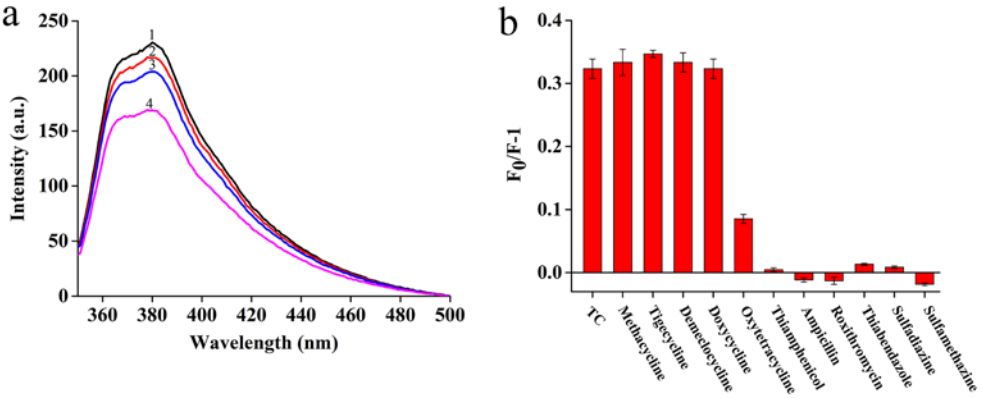

Figure 3. (**a**) Fluorescence spectra of the AdaPOF suspension solution after adding TC–methanol solution at different concentrations (curves 1–4 represent TC concentrations of 0, 0.1, 0.5 and 1.0 μmol/L, respectively; λex = 334 nm); (**b**) Study on the selectivity of AdaPOF (c_{AdaPOF} = 0.15 mg/mL; $c_{antibiotics}$ = 1.0 μmol/L, λex = 334 nm).

3.3. Possible Mechanism

To investigate the fluorescence quenching mechanism of the sensor with TC, the fluorescence lifetime measurements were performed in the presence and absence of different concentrations of TC. As shown in Figure 4a and Table S1, when TC is not present, the average fluorescence lifetime of the AdaPOF was 1.51 ns, and when TC concentration was

0.1, 1.0 and 9.0 μmol/L, the average fluorescence lifetime of the AdaPOF was 1.52, 1.53 and 1.51 ns, respectively. The results showed that the fluorescence lifetime change in AdaPOF was negligible in the presence and absence of TC, which indicated that the fluorescence quenching of the sensor proved to be a static quenching mechanism [30,31]. Moreover, the UV–vis spectrum of TC exhibited a degree of overlap with the emission spectrum of AdaPOF (Figure 4b), and thus the fluorescence quenching phenomenon of AdaPOF might be caused by the fluorescence resonance energy transfer between them [32,33].

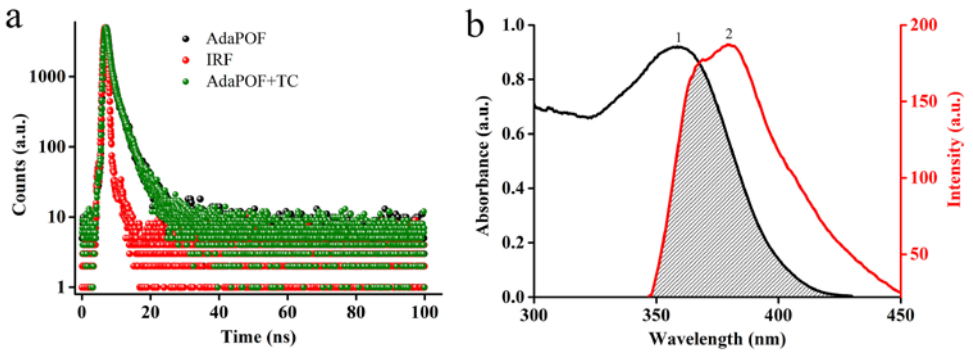

Figure 4. (**a**) The fluorescence lifetime of the AdaPOF suspension solution before and after TC–methanol solution addition (λex = 334 nm, *c* = 1.0 μmol/L); (**b**) The UV–vis spectrum of TC (curve 1) and emission spectrum of AdaPOF (curve 2).

Density functional theory (DFT) calculations were performed to further explain the selectivity behavior of TC by AdaPOF–based sensor. Based on the literature [34,35], when the sensor had a higher LUMO energy level than the analytes, the efficient electron transfer from the sensor to the analytes occurred, which was considered to be a key reason causing the fluorescence quenching process. As exhibited in Figure 5, the AdaPOF LUMO energy level (−1.10 eV) is higher than that of sulfadiazine, thiabendazole, oxytetracycline and TC. Efficient electron transfer occurred between the AdaPOF and these antibiotics, and thus the fluorescence of the sensor was quenched. At the same time, the LUMO energy state difference between AdaPOF and TC was the largest. Therefore, TC displayed a strong quenching effect toward the sensor based on AdaPOF. Moreover, it is noteworthy that roxithromycin, ampicillin and sulfamethazine had higher LUMO energy levels than AdaPOF, so these three antibiotics could not cause the sensor to produce the fluorescence quenching phenomenon.

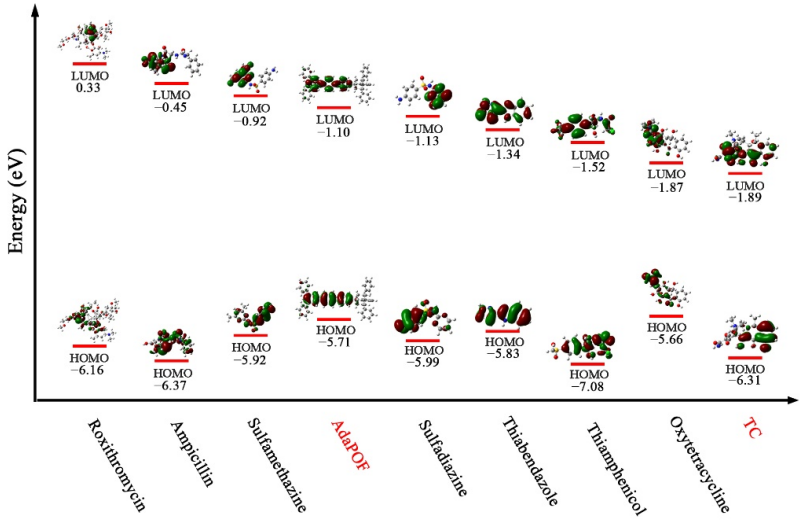

Figure 5. HOMO–LUMO energy profiles of AdaPOF and antibiotics.

3.4. Optimization of Fluorescence Sensor

The fluorescence quenching efficiency of the AdaPOF–based sensor closely relied on the experimental conditions. Here, the suspension concentration and the incubation time were carefully studied, and the results were shown in Figure 6. It can be seen from Figure 6a that the fluorescence quenching effect increased obviously at the suspension concentration from 0.05 to 0.15 mg/mL, whereas a further increase in the suspension concentration from 0.15 to 0.25 mg/mL leads to a sharp decrease in fluorescence quenching effect. The reason for this could be that, with the increase in suspension concentration, the active sites between AdaPOF and TC increase, and the fluorescence quenching effect increases. However, at a high suspension concentration, the AdaPOF would settle, resulting in the decrease in fluorescence quenching effect. Therefore, the suspension concentration of 0.15 mg/mL was chosen as TC determination condition. The incubation time was also optimized, and the result was shown in Figure 6b. When TC was added into the AdaPOF suspension, the fluorescence quenching effect increased rapidly from 0 to 20 s, and there was no obvious change after the increase in the incubation time to 16 s. Thus, 20 s was chosen as the optimum incubation time for the following experiments.

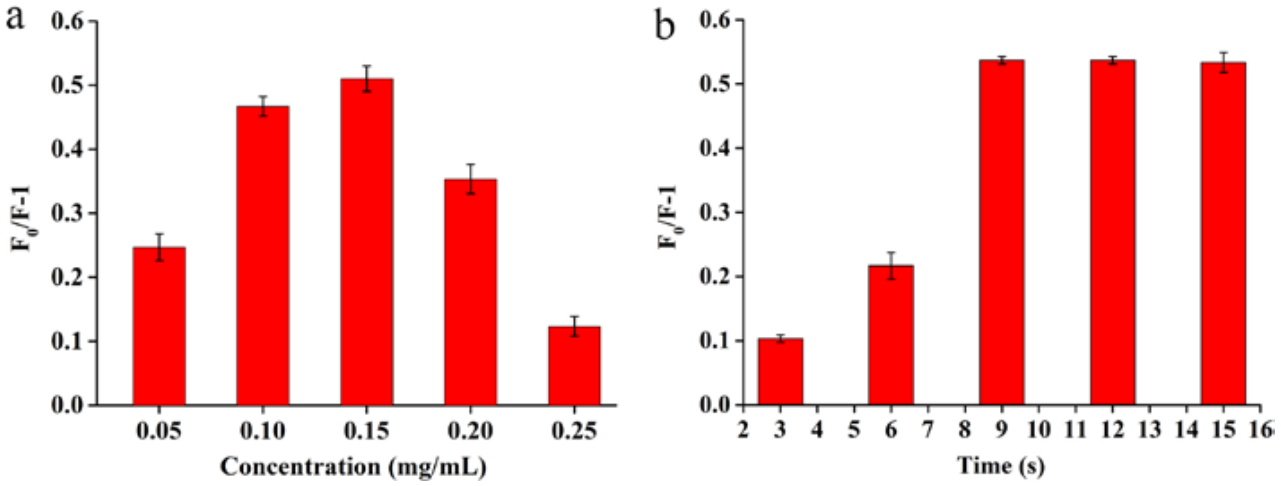

Figure 6. (**a**) Optimization of AdaPOF dichloromethane suspension concentration; (**b**) Optimization of incubation time between AdaPOF dichloromethane suspension and TC. (λex = 334 nm, *c* = 3.0 μmol/L).

3.5. Analytic Characteristics of the AdaPOF–Based Fluorescence Sensor

Under the optimized conditions, a series of TC solutions at different concentrations were added to the AdaPOF suspension solution, and the fluorescence emissions at 380 nm were recorded. Figure 7a shows that with the increase in the concentration of TC, the fluorescence emission intensity of the sensor at 380 nm was decreased gradually. The fluorescence emission intensity of the sensor quenched greatly when the concentration of TC was 9.0 μmol/L, with a quenching efficiency of 74%. As shown in Figure 7b, there was a good linear relationship between the F_0/F-1 value and the concentration of TC in the range of 0.1 to 9.0 μmol/L. The equation of linear regression was F_0/F-1 = 0.06 + 0.17*C*, where F_0 and *F* represented the fluorescence intensity in the absence and presence of TC, and *C* represented the TC concentration. The linear dependence coefficient (R^2) was 0.9959 and the limit of detection (LOD, *S*/*N* = 3) of 43 nmol/L was estimated for TC determination.

In order to prove the anti-interference performance of the fluorescence sensor for TC determination, the fluorescence intensity of the sensor from TC with different possible interferences was tested, and the obtained data were analyzed based on the change in F_0/F-1. In Figure 7c, all these possible interferences exhibited a negligible interference on fluorescence quenching effect (change less than 8%) when mixing 3.0 μmol/L TC with 500-flod K^+, Mg^{2+} and Cl^-, 200-fold Na^+, OH^-, glucose and urea, 100-fold ascorbic acid

and inositol, 40-fold NO^{3-} or 20-fold Zn^{2+}, vitamin B1 and glycine. In addition, when 20–fold quantities of all the anti-substances were added at the same time, the sensor based on AdaPOF also showed a good anti-interference performance. Therefore, the sensor based on AdaPOF had a good anti-interference performance for TC determination.

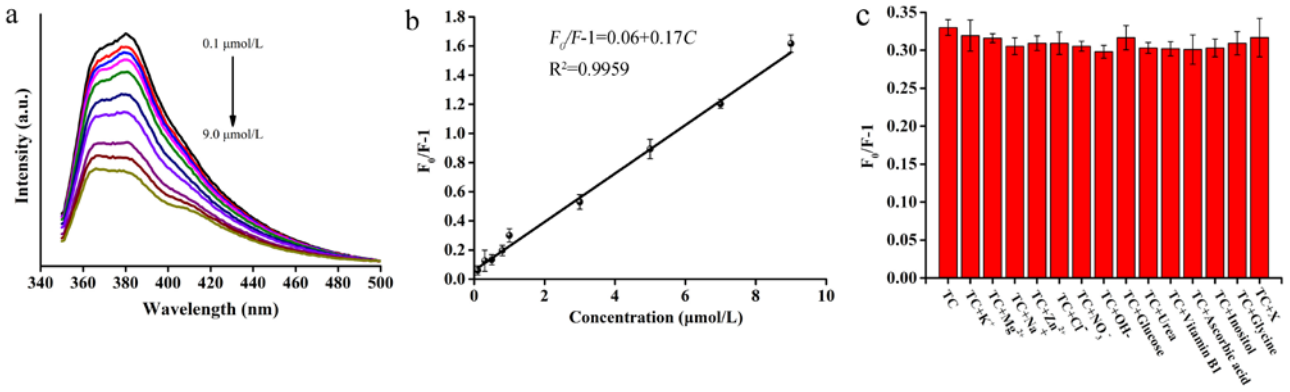

Figure 7. (**a**) Fluorescence spectra of the AdaPOF dichloromethane suspension after adding TC–methanol solution of different concentrations (λex = 334 nm); (**b**) The liner calibration curve for the determination of TC concentration; (**c**) The influence of coexisting ions or compounds on the determination of TC by AdaPOF (X = K^+, Mg^{2+}, Na^+, Zn^{2+}, Cl^-, NO^{3-}, OH^-, glucose, urea, vitamin B1, ascorbic acid, inositol and glycine). (λex = 334 nm, c = 1.0 μmol/L).

3.6. Samples Analysis

The practicability of the AdaPOF–based fluorescence method was proved by determination of TC in aquatic products, including fish, shrimp and crab. As displayed in Table 1, 0.09 mg/L of TC residual was obtained in the fish samples, while no TC was detected in the shrimp and crab. The proposed fluorescence method was also applied for analysis of these three dead aquatic products spiked with TC before sample pretreatment. The recoveries of TC in these samples were from 94.4% to 103.8%, with RSDs less than 5.0%, by the standard addition method. Moreover, these three samples were also analyzed by the HPLC method. The relative errors of the two methods were −7.6% and 6.7%. Moreover, the obtained results were also assessed by *t*-test statistical analysis, and the results showed that there was no significant difference in TC determination between these two methods (Table 1). These results suggested that the proposed fluorescence method was applicable for the determination of TC in aquatic samples. In addition, compared with the previous literatures on the analyzed of TC, as shown in Table 2, the AdaPOF–based fluorescence method exhibited either a lower LOD or a wider linear range.

Table 1. Determination of tetracycline in fish, shrimp and crab samples.

Samples	The Proposed Method					HPLC Method [b]		Relative Error [c] (%)	*t* Test Value *p* [d]
	Original (mg/L)	Spiked (mg/L)	Found (mg/L)	Recovery (%)	RSD (%, *n* = 3)	Original (mg/L)	RSD (%, *n* = 3)		
Fish	0.09	0.18	0.26	96.2	4.6	0.08	4.2	−7.6	0.60
		0.36	0.46	102.2	1.8				
Shrimp	- [a]	0.18	0.17	94.4	3.1	-	-	-	-
		0.36	0.35	97.2	2.4				
Crab	0.16	0.18	0.33	97.1	1.2	0.15	3.8	−6.7	0.43
		0.36	0.54	103.8	4.9				

[a]: no detected; [b]: The analytical separations were achieved using a reverse phase C18 column. The mobile phase was acetonitrile and 1.2 mg/L NaH_2PO_4 (26:74, *v*/*v*-), the flow rate was 1.0 mL/min and the detection wavelength was 355 nm; [c]: $(I_{\text{proposed method}} - I_{\text{HPLC}})/I_{\text{HPLC}}$, *I* represents test result; [d]: value of *t* test in the table with confident interval 95%; $p > 0.05$ indicating no significant difference.

Table 2. Comparisons of different fluorescence methods in the determination of tetracycline.

Materials	Linear Range (μmol/L)	LOD (nmol/L)	Samples	Ref.
Carbon dots	10.0–400.0	6000	Tetracycline tablets	[36]
Carbon dots	0.5–25	165	Urine	[37]
RhB [a] @ZIF–8	0–46	110	Source and tap water	[38]
TA–CuNCs@CTAB [b]	5–50; 50–130	65	Water	[39]
Carbon dots	0–350	170	Milk and milk powder	[40]
AdaPOF	0.1–9.0	43	Fish, shrimp, crab	This work

[a]: rhodamine B; [b]: cetyltrimethylammonium bromide.

4. Conclusions

To summarize, the three-dimensional AdaPOF fluorescence sensor was developed for rapid TC determination. The proposed AdaPOF was synthesized by a Suzuki coupling reaction in one step, and proved to have a large specific surface area, good thermal stability, as well as excellent fluorescent performance. Moreover, the AdaPOF shows a selective fluorescence quenching effect towards TC. The effective electron transfer between AdaPOF framework and TC constitutes the possible sensing mechanism. Furthermore, the established AdaPOF–based fluorescence method for TC determination has a range of 0.1–9.0 μmol/L and a LOD of 43 nmol/L (S/N = 3). In addition, the fluorescence method was applied to TC determination in aquatic samples, and the recoveries ranged from 94.4% to 103.8%. The results obtained by this fluorescence method were consistent with those of HPLC method in the TC determination, which demonstrated that the fluorescence method was reliable and accurate.

Supplementary Materials: The following supporting information can be downloaded at: https://www.mdpi.com/article/10.3390/chemosensors10110457/s1, Figures S1–S6 and Table S1.

Author Contributions: Z.L.: Methodology, Material synthesis, Data curation, Investigation, Writing—original draft preparation.; Y.H.: Visualization, Funding acquisition.; G.L.: Visualization, Resources, Funding acquisition, Supervision, Project administration, Writing—review and editing. L.X.: Visualization, Resources, Writing—review and editing. All authors have read and agreed to the published version of the manuscript.

Funding: The work was supported by the National Key Research and Development Program of China (No. 2019YFC1606101), the Research and Development Plan for Key Areas of Food Safety in Guangdong Province of China (No. 2019B020211001), the State Key Program of National Natural Science foundation of China (No. 22134007), and the National Natural Science Foundation of China (No. 21976213). All authors have read and agreed to the published version of the manuscript.

Institutional Review Board Statement: Not applicable.

Informed Consent Statement: Not applicable.

Data Availability Statement: Not applicable.

Conflicts of Interest: The authors declare no conflict of interest.

References

1. Li, R.X.; Wang, W.J.; El-Sayed, E.S.M.; Su, K.Z.; He, P.L.; Yuan, D.Q. Ratiometric fluorescence detection of tetracycline antibiotic based on a polynuclear lanthanide metal–organic framework. *Sens. Actuators B Chem.* **2021**, *330*, 129314. [CrossRef]
2. Li, Y.Y.; Du, Q.Q.; Zhang, X.D.; Huang, Y.M. Ratiometric detection of tetracycline based on gold nanocluster enhanced Eu^{3+} fluorescence. *Talanta* **2020**, *206*, 120202. [CrossRef]
3. Sreejith, S.; Shajahan, S.; Prathiush, P.R.; Anjana, V.M.; Viswanathan, A.; Chandran, V.; Ajith, G.S.; Jayachandran, R.; Mathew, J.; Radhakrishnan, K. Healthy broilers disseminate antibiotic resistance in response to tetracycline input in feed concentrates. *Microb. Pathog.* **2020**, *149*, 104562. [CrossRef]
4. Chen, Z.J.; Guo, H.; Liu, H.Y.; Niu, C.G.; Huang, D.W.; Yang, Y.Y.; Liang, C.; Li, L.; Li, J.C. Construction of dual *s*-scheme $Ag_2CO_3/Bi_4O_5I_2$/g-C_3N_4 heterostructure photocatalyst with enhanced visible-light photocatalytic degradation for tetracycline. *Chem. Eng. J.* **2022**, *438*, 135471. [CrossRef]

5. Feng, M.X.; Wang, G.N.; Yang, K.; Lui, H.Z.; Wang, J.P. Molecularly imprinted polymer-high performance liquidchromatography for the determination of tetracycline drugs in animalderived foods. *Food Control* **2016**, *69*, 171–176. [CrossRef]
6. Pang, Y.H.; Lv, Z.Y.; Sun, J.C.; Yang, C.; Shen, X.F. Collaborative compounding of metal–organic frameworks for dispersive. solid-phase extraction HPLC–MS/MS determination of tetracyclines in honey. *Food Chem.* **2021**, *355*, 129411. [CrossRef]
7. Zhou, J.J.; Xu, Z.Q. Simultaneous separation of 12 different classes of antibiotics under the condition of complete protonation by capillary electrophoresis-coupled contactless conductivity detection. *Anal. Methods* **2022**, *14*, 174. [CrossRef]
8. Jia, T.T.; Li, Y.S.; Niu, H.W. Recent progress in fluorescent probes for diabetes visualization and drug therapy. *Chemosensors* **2022**, *10*, 280. [CrossRef]
9. Tran, V.T.; Ju, H. Fluorescence enhancement via dual coupling of dye molecules with silver nanostructures. *Chemosensors* **2021**, *9*, 217. [CrossRef]
10. Liu, X.F.; Song, J.X.; Wang, C.; Yang, R.N.; Sun, P.F.; Huang, Y.Q.; Zhang, L.; Fan, Q.L. An amplified fluorescence biosensor for intracellular telomerase determination and in situ imaging based on thioflavin T and conjugated polymer nanoparticles. *Sens. Actuators B Chem.* **2022**, *371*, 132485. [CrossRef]
11. Ma, Q.; Gao, Z.Q.; Dayal, H.; Li, S.F.Y. A label-free fluorescent sensor based on the formation of poly(thymine)-templated copper nanoparticles for the sensitive and selective detection of microRNA from cancer cells. *Chemosensors* **2020**, *8*, 52. [CrossRef]
12. Wang, X.Y.; Yin, H.Q.; Yin, X.B. MOF@COFs with strong multiemission for diffffferentiation and ratiometric fluorescence detection. *ACS Appl. Mater. Inter.* **2020**, *12*, 20973–20981. [CrossRef] [PubMed]
13. Liang, Y.M.; Yang, H.; Zhou, B.; Chen, Y.; Yang, M.; Wei, K.S.; Yan, F.Y.; Kang, C. Waste tobacco leaves derived carbon dots for tetracycline detection: Improving quantitative accuracy with the aid of chemometric model. *Anal. Chim. Acta.* **2022**, *1191*, 339269. [CrossRef] [PubMed]
14. Chen, J.; Xu, Y.L.; Li, S.Y.; Xu, F.H.; Zhang, Q. Ratio fluorescence detection of tetracycline by a Eu^{3+}/NH_2-MIL-53(Al) composite. *RSC Adv.* **2021**, *11*, 2397. [CrossRef] [PubMed]
15. Yang, C.Y.; Bie, J.X.; Zhang, X.M.; Yan, C.Y.; Li, H.J.; Zhang, M.H.; Su, R.F.; Zhang, X.G.; Sun, C.Y. A label-free aptasensor for the detection of tetracycline based on the luminescence of SYBR Green I. *Spectrochim. Acta A* **2018**, *202*, 382–388. [CrossRef]
16. Xu, Y.L.; Wei, J.H.; Chen, X.W. Visible light-responsive sulfone-based covalent organic framework as metal-free nanoenzyme for visual colorimetric determination of uranium. *Chemosensors* **2022**, *10*, 248. [CrossRef]
17. Hu, K.; Lv, Y.X.; Ye, F.G.; Chen, T.; Zhao, S.L. Boric-acid-functionalized covalent organic framework for specifific enrichment and direct detection of *cis*-diol-containing compounds by matrix-assisted laser desorption/ionization time-of-flight mass spectrometry. *Anal. Chem.* **2019**, *91*, 6353–6362. [CrossRef]
18. Zensen, T.; Roper, T.; Fuchs, T.; Sackers, N.; Bachmann, S.; Poppler, A.C.; Jupke, A.; Palkovits, R.; Delidovich, I. Porous organic frameworks for preferable adsorption of trans-1,2-diols over cis-1,2-diols. *Appl. Mater. Today* **2022**, *28*, 101523. [CrossRef]
19. Yin, H.Q.; Yin, F.F.; Yin, X.B. Strong dual emission in covalent organic frameworks induced by ESIPT. *Chem. Sci.* **2019**, *10*, 11103. [CrossRef]
20. Chen, S.H.; Wu, Y.; Zhang, W.X.; Wang, S.S.; Yan, T.; He, S.J.; Yang, B.L.; Ma, H.P. A 3D ultramicroporous porous organic frameworks for SO2 and aromatic sulfides capture with high capacity and selectivity. *Chem. Eng. J.* **2022**, *429*, 132480. [CrossRef]
21. Lu, Z.Y.; Li, G.K.; Hu, Y.F. A Tb^{3+} functionalized triazine-porous organic framework as a ratiometric fluorescent sensor for determination of ciprofloxacin in aquatic products. *New J. Chem.* **2022**. [CrossRef]
22. Gui, B.; Lin, G.Q.; Ding, H.M.; Gao, C.; Mal, A.; Wang, C. Three-dimensional covalent organic frameworks: From topology design to applications. *Acc. Chem. Res.* **2020**, *53*, 2225–2234. [CrossRef] [PubMed]
23. Hou, B.; Yang, S.; Yang, K.W.; Han, X.; Tang, X.H.; Liu, Y.; Jiang, J.W.; Cui, Y. Confinement-driven enantioselectivity in 3D porous chiral covalent organic frameworks. *Angew. Chem. Int. Edit.* **2021**, *60*, 2–10. [CrossRef] [PubMed]
24. Nguyen, H.L.; Gropp, C.; Ma, Y.H.; Zhu, C.H.; Yaghi, O.M. 3D covalent organic frameworks selectively crystallized through conformational design. *J. Am. Chem. Soc.* **2020**, *142*, 20335–20339. [CrossRef] [PubMed]
25. Dong, J.Q.; Tummanapelli, A.K.; Li, X.; Ying, S.M.; Hirao, H.; Zhao, D. Fluorescent porous organic frameworks containing molecular rotors for size-selective recognition. *Chem. Mater.* **2016**, *28*, 7889–7897. [CrossRef]
26. Frisch, M.J.; Trucks, G.W.; Schlegel, H.B.; Scuseria, G.E.; Robb, M.A.; Cheeseman, J.R.; Scalmani, G.; Barone, V.; Petersson, G.A.; Nakatsuji, H.; et al. *Gaussian 09*; Revision a. 02; Gaussian. Inc.: Wallingford, CT, USA, 2009.
27. Dong, J.Q.; Qiao, Z.W.; Pan, Y.T.; Peh, S.B.; Yuan, Y.D.; Wang, Y.X.; Zhai, L.Z.; Yuan, H.Y.; Cheng, Y.D.; Liang, H.; et al. Encapsulation and protection of ultrathin two-dimensional porous organic nanosheets within biocompatible metal-organic frameworks for live-cell imaging. *Chem. Mater.* **2019**, *31*, 4897–4912. [CrossRef]
28. Dong, J.Q.; Li, X.; Zhang, K.; Yuan, Y.D.; Wang, Y.X.; Zhai, L.Z.; Liu, G.L.; Yung, D.Q.; Jiang, J.W.; Zhao, D. Confifinement of aggregation-induced emission molecular rotors in ultrathin two-dimensional porous organic nanosheets for enhanced molecular recognition. *J. Am. Chem. Soc.* **2018**, *140*, 4035–4046. [CrossRef]
29. Geng, T.M.; Zhu, Z.M.; Zhang, W.Y.; Wang, Y. A nitrogen-rich fluorescent conjugated microporous polymer with triazine and triphenylamine units for high iodine capture and nitro aromatic compound detection. *J. Mater. Chem. A* **2017**, *5*, 7612. [CrossRef]
30. Parshi, N.; Pan, D.; Jana, B.; Ganguly, J. Interesting static quenching of fluorescent hydrogel caused by immobilization of Cd^{2+} ions within interstitial morphology. *Sens. Actuators B Chem.* **2021**, *331*, 129419. [CrossRef]
31. Jiao, Z.H.; Hou, S.L.; Kang, X.M.; Yang, X.P.; Zhao, B. Recyclable luminescence sensor for dinotefuran in water by stable. Cadmium-organic framework. *Anal. Chem.* **2021**, *93*, 6599–6603. [CrossRef]

32. Li, J.X.; Yu, B.Q.; Fan, L.H.; Wang, L.; Zhao, Y.C.; Sun, C.Y.; Li, W.J.; Chang, Z.D. A novel multifunctional Tb-MOFfluorescent probe displaying excellent abilities for highly selective detection of Fe^{3+}, $Cr_2O_7^{2-}$ and acetylacetone. *J. Solid. State Chem.* **2022**, *306*, 122782. [CrossRef]
33. Su, P.C.; Zhang, A.R.; Yu, L.; Ge, H.W.; Wang, N.; Huang, S.Y.; Ai, Y.J.; Wang, X.K.; Wang, S.H. Dual-functional UiO-type metal-organic frameworks for the sensitive sensing and effective removal of nitrofurans from water. *Sens. Actuators B Chem.* **2022**, *350*, 130865. [CrossRef]
34. Pan, H.; Wang, S.F.; Dao, X.Y.; Ni, Y.H. Fluorescent Zn-PDC/Tb^{3+} Coordination Polymer Nanostructure: A Candidate for Highly Selective Detections of Cefifixime Antibiotic and Acetone in Aqueous System. *Inorg. Chem.* **2018**, *57*, 1417–1425. [CrossRef] [PubMed]
35. Mallick, A.; Garai, B.; Addicoat, M.A.; Petkov, P.S.; Heine, T.; Banerjee, R. Solid state organic amine detection in a photochromic porous metal organic framework. *Chem. Sci.* **2015**, *6*, 1420. [CrossRef] [PubMed]
36. Yan, Y.; Liu, J.H.; Li, R.S.; Li, Y.F.; Huang, C.Z.; Zhen, S.J. Carbon dots synthesized at room temperature for detection of tetracycline hydrochloride. *Anal. Chim. Acta* **2019**, *1063*, 144–151. [CrossRef]
37. Uriarte, D.; Domini, C.; Garrido, M. New carbon dots based on glycerol and urea and its application in the determination of tetracycline in urine samples. *Talanta* **2019**, *201*, 143–148. [CrossRef]
38. Zhang, Y.Q.; Wu, X.H.; Mao, S.; Tao, W.Q.; Li, Z. Highly luminescent sensing for nitrofurans and tetracyclines in water based on zeolitic imidazolate framework-8 incorporated with dyes. *Talanta* **2019**, *204*, 344–352. [CrossRef]
39. Zheng, X.; Chen, Q.M.; Zhang, Z.X.; Wang, Z.L.; Gong, Z.J. An aggregation-induced emission copper nanoclusters fluorescence probe for the sensitive detection of tetracycline. *Microchem. J.* **2022**, *180*, 107570. [CrossRef]
40. Hu, Y.Y.; Guan, R.T.; Zhang, S.; Fan, X.Y.; Liu, W.J.; Zhang, K.Y.; Shao, X.D.; Li, X.; Yue, Q.L. A convenient fluorescence sensor of tetracycline based on B, N codoped carbon dots/polymer composite film. *Food Chem.* **2022**, *372*, 131287. [CrossRef]